Elucidating the role of matrix stiffness in 3D cell migration and remodeling

Ehrbar, M ; Sala, A ; Lienemann, P ; Ranga, A ; Mosiewicz, K ; Bittermann, A ; Rizzi, S C ; Weber, Franz E ; Lutolf, M P

Abstract: Reductionist in vitro model systems which mimic specific extracellular matrix functions in a highly controlled manner, termed artificial extracellular matrices (aECM), have increasingly been used to elucidate the role of cell-ECM interactions in regulating cell fate. To better understand the interplay of biophysical and biochemical effectors in controlling three-dimensional cell migration, a poly(ethylene glycol)-based aECM platform was used in this study to explore the influence of matrix cross-linking density, represented here by stiffness, on cell migration in vitro and in vivo. In vitro, the migration behavior of single preosteoblastic cells within hydrogels of varying stiffness and susceptibilities to degradation by matrix metalloproteases was assessed by time-lapse microscopy. Migration behavior was seen to be strongly dependent on matrix stiffness, with two regimes identified: a nonproteolytic migration mode dominating at relatively low matrix stiffness and proteolytic migration at higher stiffness. Subsequent in vivo experiments revealed a similar stiffness dependence of matrix remodeling, albeit less sensitive to the matrix metalloprotease sensitivity. Therefore, our aECM model system is well suited to unveil the role of biophysical and biochemical determinants of physiologically relevant cell migration phenomena.

DOI: https://doi.org/10.1016/j.bpj.2010.11.082

Elucidating the role of matrix stiffness in 3D cell migration and remodeling

Running title: Matrix interactions in 3D cell migration

M. Ehrbar[#,$,£,*], A. Sala[#, $], P. Lienemann[$], A. Ranga[§], K. Mosiewicz[§], A. Bittermann[$], S.C. Rizzi[†], F.E. Weber[#], M.P. Lutolf[§,*]

[#]Oral Biotechnology & Bioengineering, Dept. Cranio-Maxillofaicail Surgery, University Hospital Zurich, Switzerland
[$]Department of Obstetrics, University Hospital Zurich, Zurich, Switzerland
[£]Zurich Center for Integrative Human Physiology, Zurich, Switzerland
[†]QUT, Brisbane, Australia
[§]Institute of Bioengineering, Ecole Polytechnique Fédérale de Lausanne (EPFL), Lausanne, Switzerland

*Corresponding Author: Matthias P. Lutolf, Institute of Bioengineering, Bldg. AI 3138, Station 15, Ecole Polytechnique Fédérale de Lausanne (EPFL), Lausanne, E-mail: matthias.lutolf@epfl.ch, Tel: +41 (0)21 693 18 76, Fax: +41 (0)21 693 18 76. Correspondence may also be addressed to M.E. (martin.ehrbar@usz.ch)

Abstract

Reductionist in vitro model systems which mimic specific extracellular matrix functions in a highly controlled manner, termed artificial extracellular matrices (aECM), have increasingly been used to elucidate the role of cell-ECM interactions in regulating cell fate. To better understand the interplay of biophysical and biochemical effectors in controlling three-dimensional (3D) cell migration, a poly(ethylene glycol) (PEG)-based aECM platform was used in this study to explore the influence of matrix crosslinking density, represented here by stiffness, on cell migration in vitro and in vivo. In vitro, the migration behavior of single pre-osteoblastic cells within hydrogels of varying stiffness and susceptibilities to degradation by matrix metalloproteases (MMP) was assessed by time-lapse microscopy. Migration behavior was seen to be strongly dependent on matrix stiffness, with two regimes identified: a non-proteolytic migration mode dominating at relatively low matrix stiffness and proteolytic migration at higher stiffness. Subsequent in vivo experiments revealed a similar stiffness dependence of matrix remodeling, albeit less sensitive to the matrix' MMP-sensitivity. Therefore, our aECM model system is well suited to unveil the role of biophysical and biochemical determinants of physiologically relevant cell migration phenomena.

Keywords: Extracellular matrix (ECM), Hydrogel, 3D migration, Proteolysis, MMP

1. Introduction

Control of 3D cell migration within and into biomaterial scaffolds plays a pivotal role in tissue engineering. Biomaterial implants designed to attract endogenous stem/progenitor cells to the site of a tissue defect to induce regeneration need to facilitate the repopulation and remodeling of an implant by host cells, a phenomenon that is controlled by large-scale cell migration (1). The lack of sufficient cell migration is arguably one of the most significant limitations in creating large tissue-engineered constructs; indeed impaired endothelial cell invasion can lead to lack of vascularization and, ultimately, to necrosis. (2). Conversely, in biomaterials that are designed as carriers for cell delivery, encapsulated cells need to be able to leave the delivery system via extensive 3D cell migration (3). As a result of these critical biological requirements, the engineering of biomaterials having optimized 3D cell migration characteristics has gained increased attention in the biomaterials field.

The optimization of cell migration behavior within biomaterials necessitates a thorough understanding of 3D cell migration mechanisms (4, 5). Extensive research on cell migration through extracellular matrices, as it occurs in diverse tissues under physiological and pathological situations, suggests that cells can move in 3D using either proteolytic (mesenchymal) or non-proteolytic (amoeboid) strategies. In contrast to migration in 2D, cells in 3D must overcome the biophysical resistance of their surrounding milieu. In proteolytic migration, cells secrete active proteases which break down macromolecules of the ECM and thus create macroscopic cavities which allow their movement. Importantly, matrix degradation is localized to the vicinity of the cell, which is possible because some proteases, such as membrane-type matrix metalloproteases (MT-MMPs), are linked to the cell membrane. Alternatively, a number of inflammatory cell types such as lymphocytes and dendritic cells, or tumor cells, are known to utilize strategies that allow them to overcome the biophysical matrix resistance by essentially squeezing through the ECM, or deforming it, independently of proteolysis (amoeboid migration). It has also been shown that the same cell type can take advantage of both mechanisms depending on the specific ECM context (6).

Various approaches to engineering synthetic biomaterials which can support both of these types of cellular migration behaviors have been reported (1). The main focus has been on rendering materials conducive to migration through interconnected, pre-existing pores (7). More recently, biomaterials have been developed as aECM that are sensitive to the action of cell-secreted proteases. For example, peptidic substrates for MMPs or plasmin placed in the backbone of crosslinked hydrophilic polymer chains have served as cleavage sites for the degradation of the resulting co-polymer hydrogels. This simple design strategy, used in conjunction with the incorporation of integrin–binding peptide or protein components which enable cell adhesion, yields synthetic ECM analogs in which cells are able to migrate by proteolytic mechanisms.

Although aECMs are increasingly used in tissue engineering and 3D cell culture to complement naturally derived matrices such as collagen or Matrigel™ (8, 9), little is known about the interplay of the various biochemical and biophysical aECM characteristics in controlling 3D cell migration behavior (4). For example, an open key question is whether certain aECM aspects favor proteolytically or non-proteolytically mediated cell migration modes. In this work, we have addressed this question using our previously developed aECM model system formed from PEG-based macromers via the transglutaminase (TG) factor XIII (10, 11). In contrast to existing 3D cell culture matrices fabricated from naturally derived ECM components, these molecularly engineered TG-PEG gels are devoid of a microstructure and are therefore essentially non-porous. Indeed, these synthetic gels are made of a molecular meshwork consisting of flexible crosslinked polymers with a mesh size on the order of tens of nanometers. Similar to existing aECM models (e.g. (12-19)), the biochemical and biophysical properties of our TG-PEG hydrogel networks can be extensively specified, for example by

incorporating protease-sensitive peptide domains and cell-adhesive ligands, or by tuning matrix stiffness via precursor polymer architecture or concentration. By exploring the modularity of this system, we systematically probed how 3D single cell migration depends on gel stiffness, adjusted independently from matrix degradability. Surprisingly, we find that in matrices with low stiffness, single cells can overcome the resistance of the matrix by engaging in a degradation-independent 3D migration mode, suggesting the use of pre-existing or *de novo*-formed macroscopic gel defects. This finding may also highlight that apart from porosity or protease sensitivity, the engineering of gel defects in seemingly homogeneous polymer gels could be a powerful means to increase cell permissiveness in relatively dense gels.

Materials and Methods

1.1 Material and Reagents

PEG-peptide conjugates Production and characterization of different eight-arm PEG precursors containing pending factor XIIIa substrate peptides having either a glutamine acceptor substrate (*n-PEG-Gln*) or a lysine donor substrate containing a MMP-sensitive linker (*n-PEG-MMP$_{sensitive}$-Lys)* or a MMP-insensitive linker *(n-PEG-MMP$_{insensitive}$-Lys)* was performed as described elsewhere (10, 11). More information can be found in the *Supplementary Materials and Methods* file.

1.2 PEG hydrogel preparation

PEG hydrogels were formed as described elsewhere (10, 11). More information can be found and as detailed in the *Supplementary Materials and Methods* file.

1.3 PEG hydrogel characterization

Rheometry on swollen gels. Storage and loss moduli (G' and G") of swollen gels (n=4 per condition) were obtained by small strain oscillatory shear rheometry (20).
Equilibrium swelling measurements. Swollen hydrogels were weighted just prior to rheometry, and the swelling ratio Q determined as the swollen gel mass divided by the gel's dry mass (calculated from the reaction conditions).
Detection of sol fractions by HPLC. The potential presence of defects in the network architecture due to uncrosslinked PEG precursors was investigated by reverse phase high-performance liquid chromatography (RP-HPLC). First, a dilution series of unreacted PEG precursors was run on an RP-HPLC instrument using a Waters (Milford, MA, USA) C_{18} symmetry column in order to establish a standard curve of UV intensities (recorded at 220nm) as a function of PEG concentration. Then, gels (50µl volume formed at 1.5% w/v) were prepared (n=4) and each was incubated in 200µl water for 24 hours. The supernatant was then collected, run on the HPLC instrument and UV intensities were compared to the standard curve to determine the corresponding amount of unreacted polymer remaining in solution.

1.4 Cell culture

Mouse preosteoblastic cells MC3T3-E1 were purchased from American Type Culture Collection (ATCC) and grown under in MC3T3-E1 culture medium (alpha-minimal essential medium, with 10% fetal bovine serum, 100U/ml penicillin G and 100mg/ml streptomycin

GIBCO BRL, Life Technologies, Grand Island, NY, USA) under standard cell culture conditions (37°C in humidified atmosphere and 5% CO_2).

1.5 Cell encapsulation

Cells suspended in cell culture medium were added right after the FXIIIa enzyme to yield single dispersed cells at a final seeding density of 6 x10^4 cells / ml of hydrogel. Subsequently the forming matrices were slowly rotated (10min at RT) until the onset of gelation to prevent sedimentation of cells, then incubated at 37°C and 5% CO_2 for additional 30 min. and finally immersed in cell culture medium

1.6 Cell migration assay

Cell migration experiments were conducted at 37°C and 5% CO_2 and high relative humidity. Hydrogel discs containing dispersed cells were equilibrated for 4 hrs in cell culture medium and then 'glued' to the bottom of 24 well cell culture dishes by applying 10 µl of 5% hydrogel to the edge of the discs. After gelation was allowed to take place for 30 min, the samples were equilibrated for 1 hour in 1 ml of pure cell culture medium or medium that contained 50µM of the broad-range MMP inhibitor GM6001 (Chemicon). Three random (x-y-z) positions, carefully selected to be completely inside the matrix, were selected using an inverse wide-field microscope (Leica, DM IRBE) equipped with a motorized stage and focus, and a black and white camera (Hamamatsu ORKA ER). Cell spreading and migration was followed for up to 36 hours by software-controlled image acquisition (Openlab) every 15 minutes.

1.7 Statistical analysis of migration parameters

Projections of real 3D tracks were followed manually by using a "Manual Tracking" plugin in ImageJ software. The resulting x and y coordinates were used in a correlated random walk model, as described by Raeber et *al.* (17) and as detailed in the *Supplementary Materials and Methods* file.

1.8 Staining and confocal microscopy

MC3T3-E1 cells were stained for f-actin and nuclei. Samples were fixed and permeabilized in 4% paraformaldehyde containing 0.2% Triton X-100 in PBS for 20 min at 4°C. Samples were incubated for 10 min in 0.1 M glycine followed by a wash step in PBS. For f-actin staining, the gels were incubated with 0.4 U/ml rhodamine-labeled phalloidin (R-415; Molecular Probes, Eugene, OR, USA) in PBS with 1% BSA for 1 h at 4°C. After washing the samples three times for 5 min in PBS, cell nuclei were co-stained with 1 ng/µl DAPI (4',6-diamidino-2-phenylindole) (D-1306; Molecular Probes, Eugene, OR, USA) in PBS for 10 min at 4°C. Z-series of approximately 30 equidistant x-y scans at 0.272 µm intervals (63x) were acquired and processed in Imaris software (Bitplane AG, Zürich, Switzerland).

For time-lapse confocal imaging, cells were stained with PKH-26 (Sigma-Aldrich) according to the manufacturer's instructions. Fluorescently labeled cells were encapsulated in hydrogels containing covalently linked TG-Lys-FITC (24). The resulting hydrogel discs were equilibrated for 4hrs in cell culture medium and then glued to the bottom of 24 well cell culture dishes by applying 10 µl of 5% hydrogel to the edge of the discs. Z-series of approximately 100 equidistant x-y scans at 1.5 µm intervals (20x) were acquired for 8 hours at 15 min. intervals in resonant scanning mode with a Leica TCS SP5 confocal microscope and processed in Imaris software.

1.9 Animal experiments

Animal experiments were authorized by the Veterinary Authority of the Canton of Zurich. Adult female Sprague-Dawley albino rats (300-350 g) were used for bone regeneration experiments as previously described (25). More information can be found in the *Supplementary Materials and Methods* file.

2 Results

2.1 Characterization of aECM properties

Cell behavior in 3D microenvironments is largely influenced by cross-link density, degradability, porosity/topology and cell-ECM adhesion, parameters which can, at least to some extent, be fine-tuned in synthetic matrices. We produced TG-PEG hydrogel matrices (10) where swelling and viscoelastic properties were modulated by different precursor concentrations (1.5, 2, and 2.5% v/w), and where sensitivity to degradation by MMPs was modulated by the linker peptide (sensitive: Ac-FKGG↓GPQG IWGQ-ERCG-NH_2, ↓ indicates the cleavage site, or insensitive: Ac-FKGG-GPQGIAGF-ERCG-NH_2) (**Fig. 1**). The viscoelastic properties of swollen gels were determined as a function of frequency by small strain oscillatory shear rheometry (20) (**Supplementary Fig. S1**). The storage moduli (G') at a frequency of 1Hz ranged from 94±25 Pa at 1.5% to 482±77 Pa at 2.5% for MMP-sensitive gels, and from 62±32 Pa (1.5%) to 347±19 Pa (2.5%) for MMP-insensitive gels (for simplicity we refer to the 1.5% gels as 'soft', the 2.5% as 'stiff' and those formed at 2% as 'intermediate') (**Supplementary Fig. S2A**). TG-PEG hydrogels with a dry mass content during gel formation of 1.5 to 2.5% thus exhibited relatively similar elastic properties as biologically derived hydrogel networks such as collagen or fibrin at concentrations of 2 mg/ml (17). The phase angle δ (corresponding to the ratio of storage and loss modulus) of 12 ± 7° of soft gels is in the range of collagen matrices, suggesting the presence of network defects in the form of non-covalently crosslinked and therefore elastically inactive network components.

To further characterize gel properties we determined the swelling ratio Q. As expected, Q decreased with increasing precursor concentration (**Supplementary Fig. S2B**). Matrices containing MMP-sensitive peptide building blocks showed a lower swelling ratio than those with MMP-insensitive peptides. Employing the Flory-Rehner model (26), Q values allowed an estimation of the mesh size of both gel types of ca. 40 nm which is orders of magnitude below cellular 'features' (not shown). It should be noted, however, that the mesh size is a crude, averaged approximation of the gel network microstructure, which does not provide any information on the defect size distribution. We would expect that 3D cell migration would rather depend on the maximal defect size. Nevertheless, we hypothesized that 3D cell migration would only be possible by local proteolytic matrix degradation, as reported for a similar chemically crosslinked aECM system (17, 27).

Finally, to approximate the degree of defects in the gels, we evaluated the sol fraction of the networks by RP-HPLC (**Supplementary Fig. S3**). The unreacted control PEG precursor was seen to have a retention time of approximately 11.7 minutes, and the smallest detectable amount using our method was established to be 7.5µg per 100µl injection. Based on our detection limit of 7.5µg, we could evaluate whether up to 2.5% of PEG remained unreacted in solution. As we could not detect any signal from our supernatant sample injections, we conclude that no soluble PEG precursors (above our detection limit of 2.5%) were present after gelation, which is not surprising since the probability that none of the octafunctional macromer had reacted is very low.

2.2 Increasing cross-linking density impedes cell spreading

To test the influence of matrix cross-link density on 3D cell spreading, we entrapped single murine MC3T3-E1 pre-osteoblastic cells in degradable gels with variable stiffness. Representative confocal images of cells that were cultured for 24 hours revealed different morphologies in response to variable network stiffness (**Supplementary Fig. S4**). Cells in soft gels quickly adopted a spindle-shaped morphology. With increasing stiffness the morphology became less elongated and reticulate filopodia were formed. In the stiff gels, the cells generally remained round with frayed filopodia.

2.3 Increasing cross-linking density impedes cell migration

Time-lapse imaging revealed that matrix stiffness not only influenced initial cell spreading but also 3D cell migration (**Fig. 2**). The onset of migration was observed as early as 4 hours after encapsulation in soft gels whereas at higher stiffness the cells started to migrate after ca. 6 hours. Notably, the overall mobility of cells entrapped in the stiffest gels was dramatically reduced compared to the intermediate and soft gels (**Fig. 2A**). Based on time-lapse imaging, we analyzed cell displacement data and created polar plots to confirm the directional independence of cell movement (**Fig. 2B**) (17).

2.4 MMP-dependent cell migration behavior

To verify that 3D cell migration in TG-PEG hydrogels is not only dependent on matrix cross-link density but also on susceptibility to proteolytic degradation, we entrapped single cells in gels containing the peptide Ac-FKGG-GPQGIAGF-ERCG-NH_2 (28) which is not an MMP-cleavable substrate. As expected, over the course of the first 24 hours in culture cells remained completely trapped within stiff and intermediate MMP-insensitive gels (**Fig. 2C** and **2D**). Interestingly, cellular activity in non-degradable gels remained intact as was evident from protruding filopodia and pseudopodia and noticeable oscillations of cell bodies, presumably due to a mechanical deformation of the matrix. To our surprise, cells embedded in the soft MMP-insensitive gels migrated to a similar degree as cells in the soft degradable gels (**Fig. 2A** and **2B**). These data thus indicate that 3D cell migration behavior is dependent on both biochemical and biophysical matrix properties: stiffer matrices facilitated migration by proteolytic remodeling, whereas soft matrices appeared to support a MMP-insensitive migration mode.

2.5 MMP-independent cell migration behavior

To exclude that the differences in mechanical properties of MMP-sensitive and -insensitive gels (**Supplementary Fig. S2A**) were responsible for the MMP-independent migration in non-degradable gels, we performed migration experiments in the presence of the broad-range MMP-inhibitor GM 6001 (**Supplementary Fig. S5** and **S6**). Consistent with the previous data, we observed complete inhibition of 3D migration in intermediate and stiff matrices but almost no change in migration within soft gels. These results indicate that the migratory machinery is not impaired by a synthetic MMP inhibitor, but rather that cells are not able to migrate above a certain matrix stiffness. This provides further confirmation that the inability to block migration in the MMP-insensitive hydrogel is due to the low stiffness of the hydrogel rather than the proteolytic degradation of negative control peptide.

2.6 *Single cell migration parameters depend on biochemical and biophysical matrix properties*

In order to substantiate the above observations, we quantified the 3D migration rate and persistence time based on time-lapse imaging series of at least 24 consecutive time frames by applying an unbiased random walk model (17). The percentage of migrating cells was based on the persistence length criterion of L_{crit} = 1.2 μm. The histograms of the speed of migrating cells showed a rather broad and positively skewed distribution, except for soft gels (**Supplementary Fig. S7**). The average speed in MMP-sensitive hydrogels decreased significantly with stiffness, from 1 μm/min (soft) to 0.5 μm/min (intermediate) and 0.2 μm/min (stiff) gels, respectively (**Fig. 3A and Supplementary Fig. S7A**). The average migration speed within MMP-insensitive matrices remained as high as 0.5 μm/min in the soft gels and only decreased to 0.2 μm/min for the stiffer gels. These values may be due to the inaccuracy of the manual evaluation procedure as well as to the elasticity of the substrate, rather than from an effective movement of the cell body. Persistence time showed a similar trend as cell speed (**Fig. 3B and Supplementary Fig. S7B**). However, the distribution for all conditions was positively skewed. The highest persistence times were observed in the soft MMP-sensitive hydrogels, with average values of 30 min. This value is significantly larger than within intermediate (20 min) or stiff gels (5 min). The persistence time of cells in the soft MMP-sensitive and MMP-insensitive hydrogels are not significantly different, indicating that the predominant migration mode could be independent of proteolytic matrix remodeling. These data show that 3D cell migration can depend on biochemical and biophysical matrix properties (**Fig. 4 and Supplementary Fig. S8**). Hydrogels which are loosely crosslinked, resulting in relatively high swelling ratios Q (**Fig. 4A**) and low stiffness G´ (**Fig. 4B**), might permit 3D cell migration independent of the matrix' proteolytic sensitivity, for example via existing or newly formed macroscopic gel 'defects', whereas migration in relatively densely crosslinked gels strictly relies on proteolytic degradation of the elastically active macromolecules in close vicinity of the cell.

2.7 *Cell-mediated proteolytic remodeling leaves behind macroscopic 'tunnels' of digested matrix*

We next tried to assess by live cell confocal microscopy whether migration in PEG hydrogels is made possible by the formation of macroscopic channels, either generated by proteolytic digestion or by a physical mechanism (**Fig. 5**). For this purpose, single cells were fluorescently labeled with the membrane dye PKH26 and then encapsulated in *FITC-labeled* MMP-sensitive matrices formed at 1.5% precursor content, either in the absence (**Fig. 5A**) or presence (**Fig. 5B**) of the MMP inhibitor GM6001 to completely block proteolytic migration. Z-stacks of migrating cells were collected for a period of 8 hours with a time-interval of 15 minutes. 3D-reconstruction of images was performed using either a maximum intensity projection method to highlight localized matrix compression around cells (**Fig. 5A** and **B,** upper panels), or a minimum intensity projection method to highlight macroscopic matrix defects, ie. putative cell tracks (**Fig. 5A** and **B,** lower panels).

As expected, zones of bright green colour in close vicinity of the cells showing regions of higher FITC-concentration were seen, suggesting that migrating cells are exerting forces to locally deform their surrounding matrix. In contrast, in MMP-sensitive matrices in the absence of GM6001 a minimum intensity projection analysis of image stacks revealed a clearly visible network of interconnected macroscopic cavities, possibly harboring the encapsulated single cells initially, as well as micrometer-sized tracks generated by migrating cells (**Fig. 5A**). These cavities and tracks appear to be permanent and were also seen in fixed samples at higher resolution (**Fig. 5C** and **D**). The smaller cell tracks are presumably caused

by MMP-mediated digestion of the hydrogel network as is evident from an analysis of cells migrating in the presence of the MMP inhibitor (**Fig. 5B**). Although extensive migration under these conditions was observed and the larger cavities were still visible, smaller tracks caused by migrating cells had mostly disappeared. We assume that cells in the latter case cells migrate through *de novo*-created matrix defects most likely generated by a physical (e.g. rupture of the matrix) rather than a biochemical mechanism. Since the matrix is highly swellable and no material would be removed in that case, such defects could not be visualized by our method as tracks would disappear after cell displacement.

Taken together, although we cannot fully exclude the existence of pre-existing macroscopic defects (or pores) below the resolution by this microscopic evaluation, we believe that these defects are not pre-existing but rather formed by cells that squeeze through the hydrogel network and induce the propagation of defects to generate cracks sufficient for cell migration.

2.8 Formation of 3D cellular networks in vitro is dependent on matrix composition

Long-term cultures of single cells entrapped in matrices with different stiffness and MMP-sensitivity showed that matrix properties could influence the formation of 3D cellular morphogenetic structures in vitro (**Fig. 6**). In line with the above migration results, highly interconnected cellular networks that permeate all gel areas were formed after three weeks in culture in soft MMP-degradable hydrogels. With increasing stiffness the density of these cellular networks decreased, as cells were increasingly hindered from proliferating and penetrating the matrix. Remarkably, cells in soft, non-degradable gels and cells in intermediate, degradable gels formed similar morphogenetic structures, indicating that although cells efficiently penetrate the gel while migrating, this might be restricted to preferentially used gel areas. The network formation in non-degradable gels of higher crosslink density, or in gels incubated with the MMP inhibitor GM6001 (**Supplementary Fig. S9**), was almost absent, in line with the above 3D migration data.

2.9 In vivo remodeling and tissue regeneration is dependent on matrix composition

We next tested how the reported in vitro behaviors would translate to a more complex in vivo cell migration context. We chose a previously established rat bone regeneration model (25). 8-mm calvarial defects were allowed to heal in the presence of MMP-sensitive or -insensitive gel implants with different stiffness which also contained 1 μg of BMP-2. These conditions had previously been shown to induce bone healing within ca. 5 weeks (25). We reasoned that this experimental model could be explored to assess in vivo invasion of endogenous cells at early time-points (i.e. 1-3 weeks) preceding de novo bone formation.

Gels were explanted after only 2 weeks and assessed by histological analysis and μCT. Similarly to the previously characterized in vitro behavior, the in vivo recruitment of a cellular invasion ‘front’ was largely dependent on the hydrogel properties (**Fig. 7A**). Matrix stiffness appeared to be an important determinant of cell invasion in vivo. Soft gels were completely penetrated by endogenous cells and only minor quantities of detectable gel remained. With increasing stiffness, the distribution of cells within the matrices became less regular and preferential paths of multi-cellular assemblies separated by intact gel mass were often seen. At the highest stiffness, cells did not invade the hydrogel and the formation of new tissue was entirely restricted to the cell-matrix interface.

The overall remodeling kinetics of the implants was assessed by histo-morphometric determination of remaining gel mass (**Fig. 7B**). The slow remodeling of the MMP-insensitive compared to the MMP-sensitive hydrogels indicated that MMPs significantly contribute to the

remodeling process. However, the degradation by protease-independent mechanisms and/or by proteases other than MMPs cannot be excluded.

3 Discussion

The understanding and optimization of 3D cell migration within and into biomaterials scaffolds is critically important for the field of tissue engineering. Here we have utilized TG-PEG gels as a model system to shed light on the role of matrix stiffness and proteolytic remodeling on 3D cell migration in vitro and in vivo.

Structural components of the native ECM such as fibrillar collagen provide an interconnected micro-porous network intercalated with other matrix components such as glycosaminoglycans. Cell migration within this complex milieu is the net result of proteolysis-dependent and -independent mechanisms (5), a distinction that often cannot be made easily. Indeed, interpretations of cell migration data from in vivo ECMs, or in vitro models that are derived from naturally derived ECM components can be confounded by the difficulty to engineer ECM characteristics and/or to parse the various cell–ECM interactions that influence 3D cell migration in these systems. For example, Sabeh et *al.* showed that cancer cells migrate within non-covalently crosslinked collagen gels independently of proteases, while in covalently crosslinked gels, MT1-MMP was demonstrated to be indispensable (29). In contrast, engineering approaches now allow to build aECMs with very good control over the materials microstructure, in some cases to form scaffolds that are essentially amorphous and pore-free. Indeed, by using synthetic and natural protease inhibitors, some of us had previously shown that 3D migration in dense chemically crosslinked PEG hydrogels is strictly dependent on proteolysis (17, 27). Here, using enzymatically crosslinked PEG-based matrices, we expected a similar protease-dependency, across the entire stiffness range tested. We calculated molecular mesh sizes from swelling ratios of all gel conditions to be on the order of tens of nanometers and thus far below the threshold that a cell could breach to penetrate the surrounding physical matrix barrier. Indeed, cells encapsulated within relatively stiff gels, formed at 2 or 2.5% solid content, were unable to migrate in the absence of proteolytic activity, as was shown by blocking proteolysis or assessing cell migration in stable gels. However, just a slight decrease in cross-linking density, induced by changing the solid content to 1.5%, resulted in matrices through which cells were able to efficiently migrate. Although the activity of proteases other than MMPs cannot be fully excluded, our data strongly suggest protease-independent migration mechanisms under these conditions.

Besides the restriction of migration in the absence of a microscopic porosity, the viscoelastic matrix properties might also directly impact the migratory behavior of cells in 3D (4, 30-32). Studies have demonstrated that certain cell types can adopt an amoeboid mode of migration that is independent of matrix remodeling and is instead characterized by localized ECM deformation and cell shape changes (33). Such a mechanism might be strongly dependent on the biophysical properties of the microenvironment and could possibly explain our data. However, we think that this is rather unlikely. First, fibroblast-like preosteoblastic cells would be expected to migrate by a mesenchymal-type mechanism (34). Second, ameboid migration has thus far only been observed in physically crosslinked matrices that allow material displacement by cellular forces, while the PEG-based gels used here are crosslinked by much stronger covalent bonds. Alternatively, one could think of a mechanism in which cells exploit existing, macroscopic gel defects or even exert sufficiently large forces to produce local propagating ‘cracks’ within the hydrogels; unfortunately this is a hypothesis that is not easily testable. Interestingly, it is well documented that single-component hydrogels, and in particular those formed from synthetic polymers such as PEG, are

mechanically very fragile, a problem that can be overcome by choosing more sophisticated multicomponent design strategies (35). Such cracks might be accessible for migrating cells and could result in a migration speed that exceeds that of cells that rely exclusively on proteolytic migration in higher density hydrogels.

The hydrogel matrices used in vitro under well-defined culture conditions were subjected to a considerably more complex in vivo situation in order to assess the migratory events during early bone regeneration. Similarly to the in vitro situation, more densely cross-linked matrices led to marginal migration to the inside of the gel and, consequently, bone formation limited on the outside. Although differences were significant, the sensitivity of the implanted materials to MMPs seemed to play a less important role during in vivo remodeling compared to the in vitro migration model. Under in vivo conditions, many more factors influencing the gel performance come into play. For example, the amount and range of proteases could be considerably different between cell culture conditions and in a healing environment due to the interaction of the implant with a higher numbers of cells specialized in rapid remodeling in the in-vivo condition (e.g. inflammatory cell types). Nevertheless, the good correlation between in vivo and in vitro behaviors suggests that our in vitro migration model can be successfully applied to predict the response of modulated material characteristics in specific tissue regeneration applications.

Indeed, a good control over in vivo cell fates via engineered ECMs would be an extremely useful capability (36). Our results suggest that through variation of network stiffness or proteolytic susceptibility and specificity, recruited cells could be restricted to the tissue-material interface or directed to migrate into the material. In comparison to healing that relies on surface erosion, the generation of new tissue from the inside out of an implant might be considerably faster. In agreement with this notion, we generally found that the most efficient bone formation in long-term experiments occurs with gel compositions that allowed efficient cell migration. It can also be noted that soft gels which led to very fast gel degradation failed to support complete healing, presumably because the implant stability did not support bone tissue formation (unpublished data).

4 Supplementary Material

Supplemental materials to this article can be found online.

5 Acknowledgements

We thank Flora Nicholls for help with animal trials and Esther Kleiner for help with histology. This work has been supported by grants from the Swiss National Foundation (CR3213-125426/1 and 310000-116240), the European Community's Angioscaff Program contract 214402 and a EURYI grant.

6 References

1. Lutolf, M. P., and J. A. Hubbell. 2005. Synthetic biomaterials as instructive extracellular microenvironments for morphogenesis in tissue engineering. Nature Biotechnology 23:47-55.
2. Phelps, E., and A. García. 2010. Engineering more than a cell: vascularization strategies in tissue engineering. Curr Opin Biotechnol. doi:10.1016/j.copbio.2010.06.005.
3. Mooney, D. J., and H. Vandenburgh. 2008. Cell delivery mechanisms for tissue repair. Cell Stem Cell 2:205-213.
4. Zaman, M. H., P. Matsudaira, and D. A. Lauffenburger. 2007. Understanding effects of matrix protease and matrix organization on directional persistence and translational speed in three-dimensional cell migration. Annals of Biomedical Engineering 35:91-100.

5. Ilina, O., and P. Friedl. 2009. Mechanisms of collective cell migration at a glance. Journal of Cell Science 122:3203-3208.
6. Friedl, P., and K. Wolf. 2010. Plasticity of cell migration: a multiscale tuning model. Journal of Cell Biology 188:11-19.
7. Moroni, L., J. R. De Wijn, and C. A. Van Blitterswijk. 2008. Integrating novel technologies to fabricate smart scaffolds. Journal of Biomaterials Science-Polymer Edition 19:543-572.
8. Lutolf, M. P. 2009. Integration column: Artificial ECM: expanding the cell biology toolbox in 3D. Integrative Biology 1:235-241.
9. Tibbitt, M. W., and K. S. Anseth. 2009. Hydrogels as Extracellular Matrix Mimics for 3D Cell Culture. Biotechnology and Bioengineering 103:655-663.
10. Ehrbar, M., S. C. Rizzi, R. Hlushchuk, V. Djonov, A. H. Zisch, J. A. Hubbell, F. E. Weber, and M. P. Lutolf. 2007. Enzymatic formation of modular cell-instructive fibrin analogs for tissue engineering. Biomaterials 28:3856-3866.
11. Ehrbar, M., S. C. Rizzi, R. Schoenmakers, J. A. Hubbell, F. E. Weber, and M. P. Lutolf. 2007. Biomolecular hydrogels formed and degraded via site-specific enzymatic reactions. Biomacromolecules 8:3000-3007.
12. Gobin, A. S., and J. L. West. 2002. Cell migration through defined, synthetic ECM analogs. Faseb J 16:751-753.
13. Halstenberg, S., A. Panitch, S. Rizzi, H. Hall, and J. A. Hubbell. 2002. Biologically engineered protein-graft-poly(ethylene glycol) hydrogels: a cell adhesive and plasmin-degradable biosynthetic material for tissue repair. Biomacromolecules 3:710-723.
14. Bryant, S. J., and K. S. Anseth. 2002. Hydrogel properties influence ECM production by chondrocytes photoencapsulated in poly(ethylene glycol) hydrogels. J Biomed Mater Res 59:63-72.
15. Shu, X. Z., Y. Liu, F. Palumbo, and G. D. Prestwich. 2003. Disulfide-crosslinked hyaluronan-gelatin hydrogel films: a covalent mimic of the extracellular matrix for in vitro cell growth. Biomaterials 24:3825-3834.
16. Kim, S., E. H. Chung, M. Gilbert, and K. E. Healy. 2005. Synthetic MMP-13 degradable ECMs based on poly(N-isopropylacrylamide-co-acrylic acid) semi-interpenetrating polymer networks. I. Degradation and cell migration. J Biomed Mater Res A 75:73-88.
17. Raeber, G. P., M. P. Lutolf, and J. A. Hubbell. 2005. Molecularly engineered PEG hydrogels: A novel model system for proteolytically mediated cell migration. Biophysical Journal 89:1374-1388.
18. Almany, L., and D. Seliktar. 2005. Biosynthetic hydrogel scaffolds made from fibrinogen and polyetheylene glycol for 3D cell cutlures. Biomaterials 26:2467-2477.
19. Peyton, S. R., C. B. Raub, V. P. Keschrumrus, and A. J. Putnam. 2006. The use of poly(ethylene glycol) hydrogels to investigate the impact of ECM chemistry and mechanics on smooth muscle cells. Biomaterials 27:4881-4893.
20. Lutolf, M. P., and J. A. Hubbell. 2003. Synthesis and physicochemical characterization of end-linked poly(ethylene glycol)-co-peptide hydrogels formed by Michael-type addition. Biomacromolecules 4:713-722.
21. Schense, J. C., and J. A. Hubbell. 1999. Cross-linking exogenous bifunctional peptides into fibrin gels with factor XIIIa. Bioconjug Chem 10:75-81.
22. Hu, B. H., and P. B. Messersmith. 2003. Rational design of transglutaminase substrate peptides for rapid enzymatic formation of hydrogels. J Am Chem Soc 125:14298-14299.
23. Lutolf, M. P., N. Tirelli, S. Cerritelli, L. Cavalli, and J. A. Hubbell. 2001. Systematic modulation of Michael-type reactivity of thiols through the use of charged amino acids. Bioconjugate Chemistry 12:1051-1056.
24. Sala, A., M. Ehrbar, D. Trentin, R. G. Schoenmakers, J. Voros, and F. E. Weber. 2010. Enzyme Mediated Site-Specific Surface Modification. Langmuir 26:11127-11134.
25. Lutolf, M. P., F. E. Weber, H. G. Schmoekel, J. C. Schense, T. Kohler, R. Mèuller, and J. A. Hubbell. 2003. Repair of bone defects using synthetic mimetics of collagenous extracellular matrices. Nat Biotechnol 21:513-518.
26. Flory, P. J. 1953. Principles of Polymer Chemistry. UniversityPress, Ithaca, NY.
27. Raeber, G. P., M. P. Lutolf, and J. A. Hubbell. 2007. Mechanisms of 3-D migration and matrix remodeling of fibroblasts within artificial ECMs. Acta Biomaterialia 3:615-629.

28. Lutolf, M. P., J. L. Lauer-Fields, H. G. Schmoekel, A. T. Metters, F. E. Weber, G. B. Fields, and J. A. Hubbell. 2003. Synthetic matrix metalloproteinase-sensitive hydrogels for the conduction of tissue regeneration: Engineering cell-invasion characteristics. Proceedings of the National Academy of Sciences of the United States of America 100:5413-5418.
29. Sabeh, F., R. Shimizu-Hirota, and S. J. Weiss. 2009. Protease-dependent versus -independent cancer cell invasion programs: three-dimensional amoeboid movement revisited. Journal of Cell Biology 185:11-19.
30. Pedersen, J. A., and M. A. Swartz. 2005. Mechanobiology in the third dimension. Annals of Biomedical Engineering 33:1469-1490.
31. Zaman, M. H., L. M. Trapani, A. Siemeski, D. MacKellar, H. Y. Gong, R. D. Kamm, A. Wells, D. A. Lauffenburger, and P. Matsudaira. 2006. Migration of tumor cells in 3D matrices is governed by matrix stiffness along with cell-matrix adhesion and proteolysis. Proceedings Of The National Academy Of Sciences Of The United States Of America 103:10889-10894.
32. Dikovsky, D., H. Bianco-Peled, and D. Seliktar. 2008. Defining the role of matrix compliance and proteolysis in three-dimensional cell spreading and remodeling. Biophysical Journal 94:2914-2925.
33. Wolf, K., I. Mazo, H. Leung, K. Engelke, U. H. von Andrian, E. I. Deryugina, A. Y. Strongin, E. B. Brèocker, and P. Friedl. 2003. Compensation mechanism in tumor cell migration: mesenchymal-amoeboid transition after blocking of pericellular proteolysis. J Cell Biol 160:267-277.
34. Friedl, P., and E. B. Brocker. 2000. The biology of cell locomotion within three-dimensional extracellular matrix. Cellular and Molecular Life Sciences 57:41-64.
35. Gong, J. P., Y. Katsuyama, T. Kurokawa, and Y. Osada. 2003. Double-network hydrogels with extremely high mechanical strength. Advanced Materials 15:1155-+.
36. Chan, G., and D. J. Mooney. 2008. New materials for tissue engineering: towards greater control over the biological response. Trends in Biotechnology 26:382-392.

Figures

Figure 1

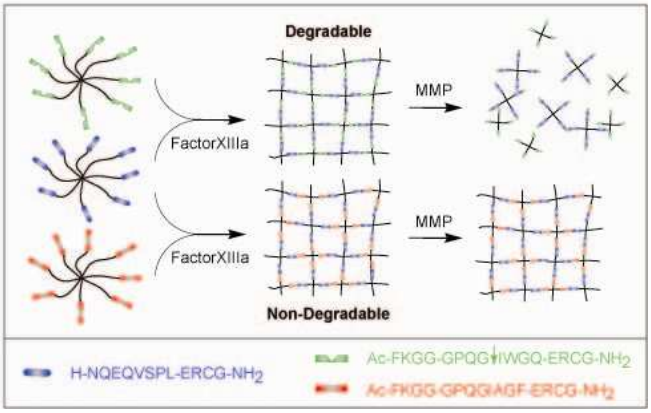

FIGURE 1 Scheme of the modular design of PEG-based aECMs. Stoichiometrically balanced ([Lys]/[Gln]=1) 8-arm PEG macromers in a buffer solution are enzymatically cross-linked via their pending glutamine acceptor [Gln] and lysine-donor [Lys] FXIIIa substrate sequences to form a hydrogel. By variation of the linker sequence and the initial precursor concentration, aECMs with different stiffness and MMP-sensitivities in presence of constant RGD concentrations can be generated.

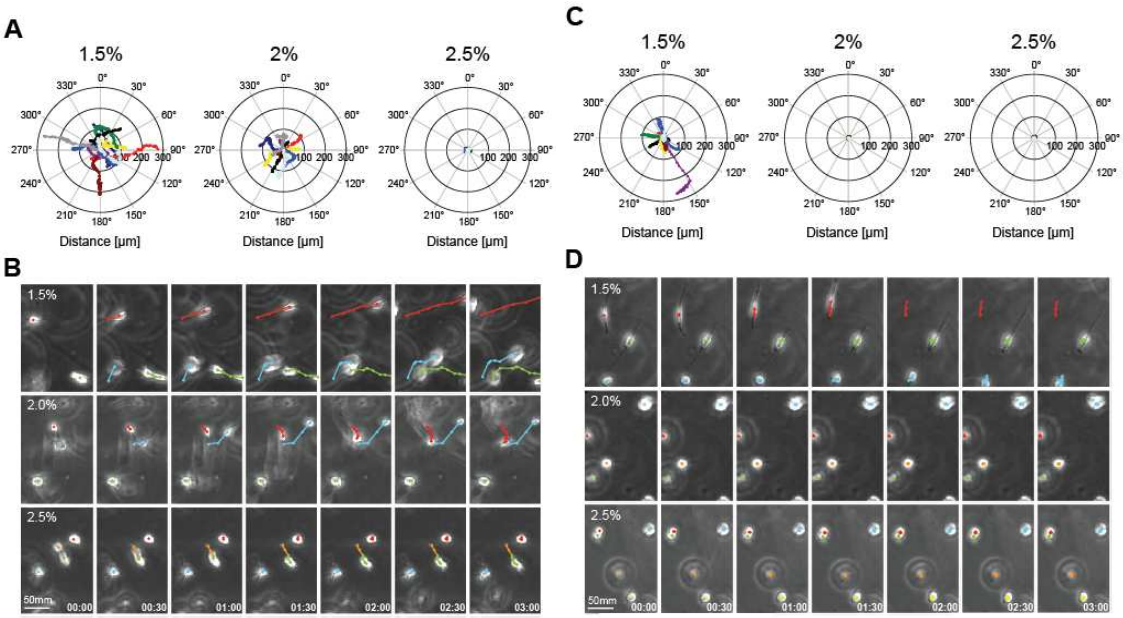

FIGURE 2 Representative track plots and time-lapse images of MC3T3-E1 cells in 3D culture. (A and B) The projection of 10 migrating cells was acquired and overlaid with a common starting point. The tracks representing a 14.5-hour period (58 x 15 min) do not show a preferred orientation. (C and D) Typical time-lapse images of cells in 3D culture (time interval t = 30 min). The track of three individual cells is indicated by the sequentially determined center of the cell. C) Efficient elongation and migration in soft MMP-sensitive hydrogels was observed that is reduced with increasing stiffness. (D) In soft MMP-insensitive hydrogels cells also migrated, whereas in intermediate or stiff gels cells remained round.

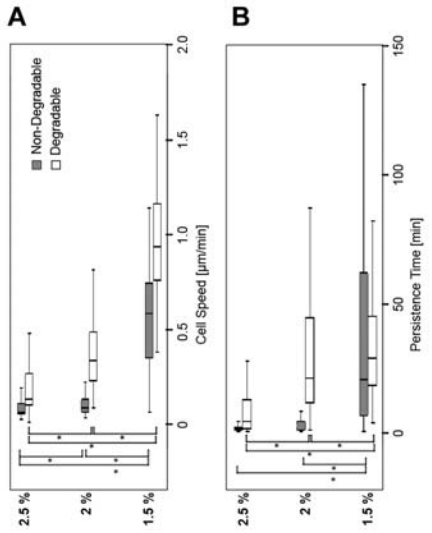

FIGURE 3 3D single cell migration as a function of gel stiffness and MMP-sensitivity. (A) Mean cell speed and (B) persistence time of all cells of a group were analyzed from time-lapse images of at least 24 consecutive time points. Values are displayed as box plots ranging from 25th to 75th percentile including the whiskers from the 10th to the 90th percentile. (A) The average cell speed and the average ((∗) $p < 0.05$) (B) persistence time decreased significantly with increasing stiffness of the matrix ((∗) $p < 0.05$). (C and D) Cells grouped in a migrating and non-migrating population based on the persistence length criterion $L_{crit} = 1.2$ µm.

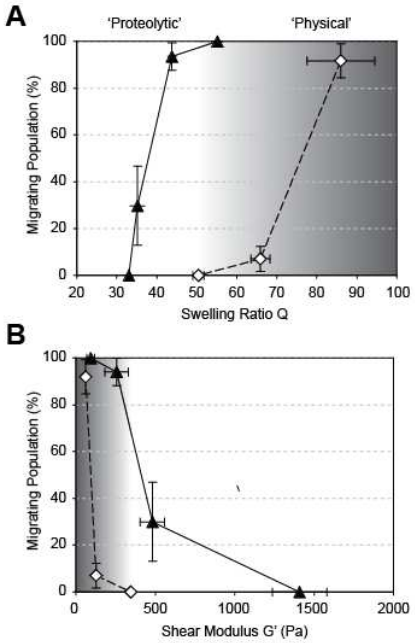

FIGURE 4 (A) The high swelling ratio Q results in a large population of migrating cells which in MMP-sensitive gels is due to mostly proteolytic matrix remodeling and in MMP-insensitive gels due to "physically" controlled cell migration. With decreasing swelling ratios the migrating population decreases. (B) In soft matrices, almost all the cells migrate in MMP-sensitive and MMP-insensitive gels. By increasing the stiffness, migration ceases and only cells in MMP-sensitive substrates can migrate.

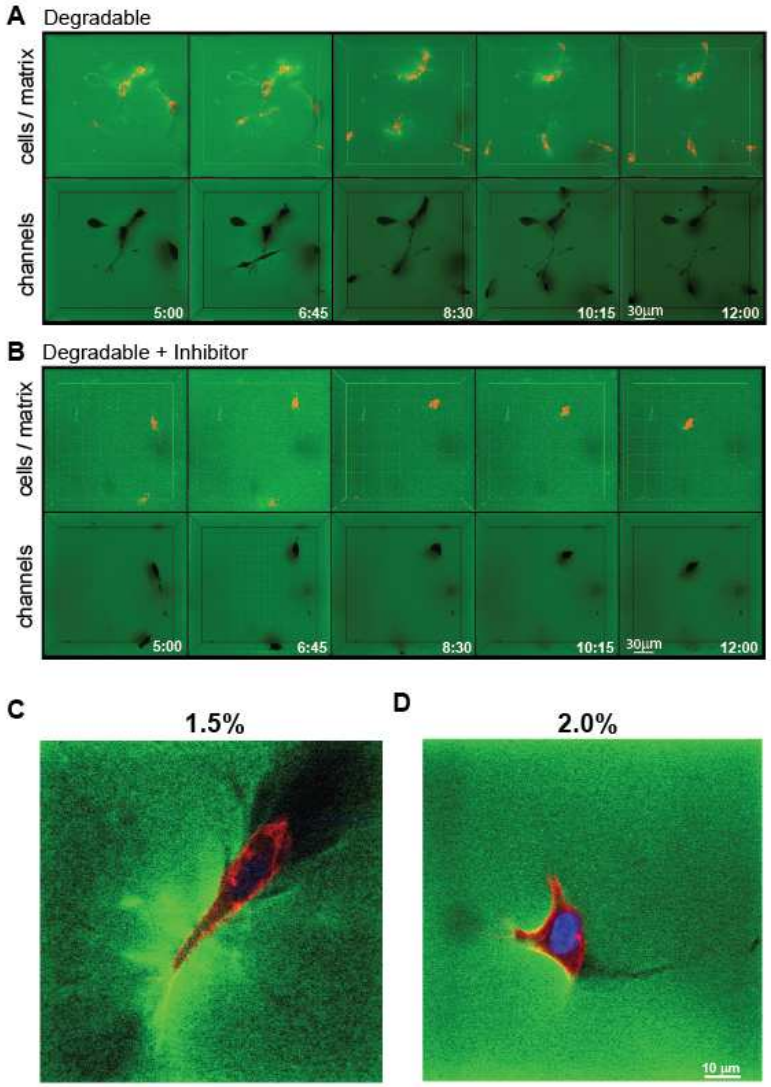

FIGURE 5 Visualization of cell-induced matrix deformation and marcroscopic cavities. (A, B) Migrating PKH26-labeled cells were encapsulated in FITC-conjugated, soft (1.5%) matrices in the absence (A) or presence (B) of GM6001 and followed by 4D time-lapse confocal microscopy for 8 hours. In both cases, 3D reconstruction of z-stacks over time in maximum intensity projection mode (cells in red/matrix in green) revealed an increase in matrix intensity (green), indicating localized matrix deformation around migrating cells. 3D reconstruction of stack from the same time points performed in minimum intensity projection mode (matrix in green) revealed the presence of a 'network' of interconnected macroscopic cavities and small cracks indicated the cell migrating paths. (C, D) High-resolution z-section of encapsulated cells within soft and intermediate degradable gels after 1 day in culture (fixed samples).

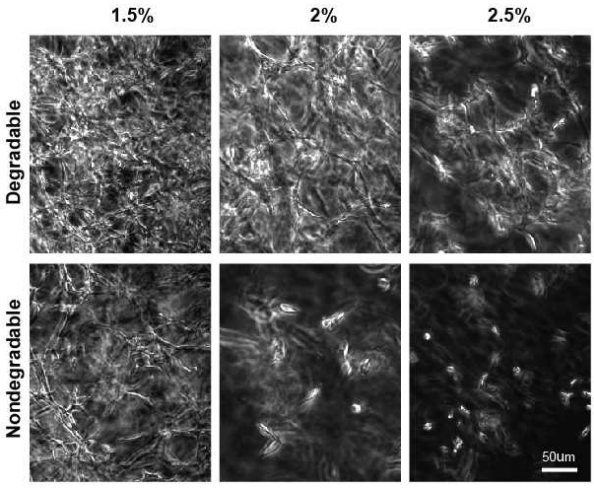

FIGURE 6 Matrix stiffness and MMP-sensitivity influence the formation of cellular networks. Starting from single cells, dense and evenly distributed cellular networks are formed in soft MMP-sensitive gels within three weeks. With increasing stiffness the cell distribution becomes less homogenous and less dense. The formation of cellular networks in MMP-insensitive soft hydrogels is largely reduced and in intermediate or stiff hydrogels is almost absent.

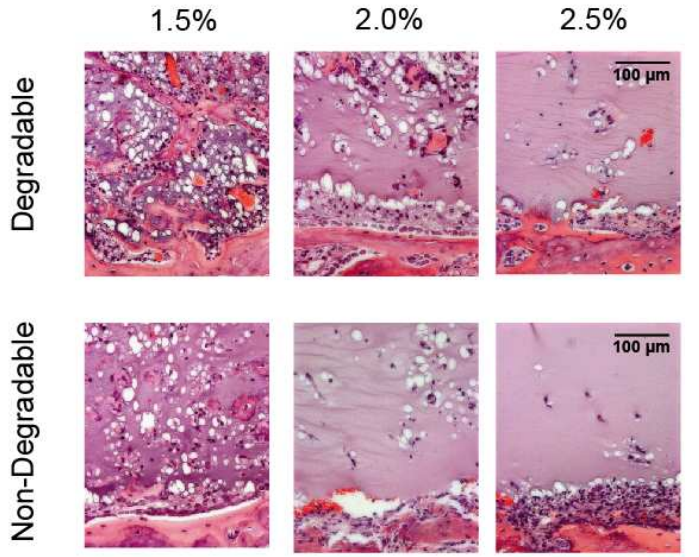

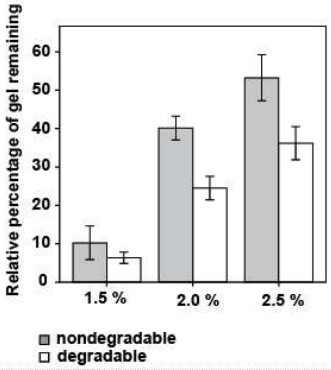

FIGURE 7 In vivo matrix remodeling is controlled by gel properties. (A) Critical-sized calvarial defects in rats were treated with soft, intermediate and stiff MMP-sensitive and -insensitive hydrogels containing 1 µg BMP-2. Samples were fixed, de-mineralized and

paraffin sections were stained with hematoxylin and eosin. Within two weeks, endogenous cells invade, degrade and remodel provisional MMP-sensitive matrices in a stiffness-dependent manner. Cell invasion is homogenous in soft gels and becomes less regular in more dense gels. MMP-insensitive gels are less efficiently invaded by cells. (n = 5) (B) The stiffness and MMP-dependent degradation rate of the aECM was confirmed by histo-morphometrical quantification of the gel leftovers. (mean ± SD, n = 5)

Supplementary Information

1. Measurement of viscoelastic and swelling properties of TG-PEG hydrogels

The mechanical properties of pre-swollen hydrogels were measured by frequency sweeps from 0.1 to 10 Hz. G´, G´´, and the phase angle were typically constant in the frequency range from 0.1 to 1 Hz and at higher frequencies started to increase. G´ was observed to be two orders of magnitude larger than G´´.

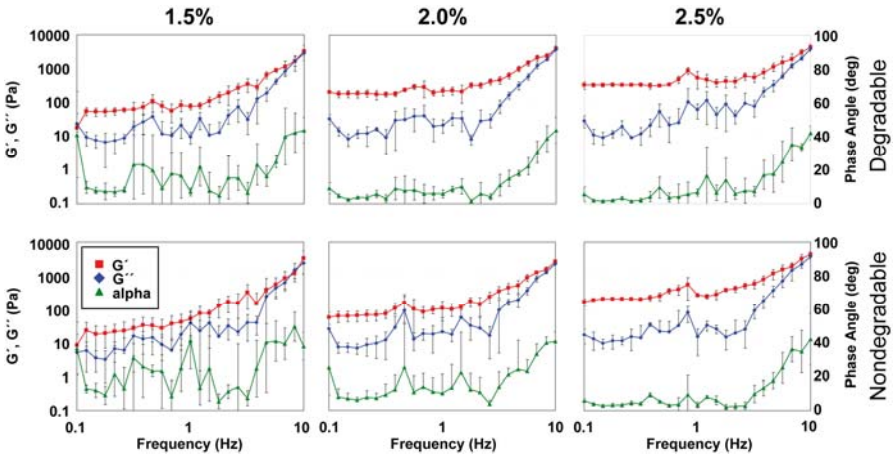

Figure S1. Typical mechanical spectra for swollen gels formed at different (w/v) precursor concentrations. G´ was constant at the low frequency range (0.1-1 Hz), and G´´ was generally around 2 orders of magnitude smaller than G´. G´´, G´ and the phase angle were seen to increase at frequencies higher than 1 Hz.

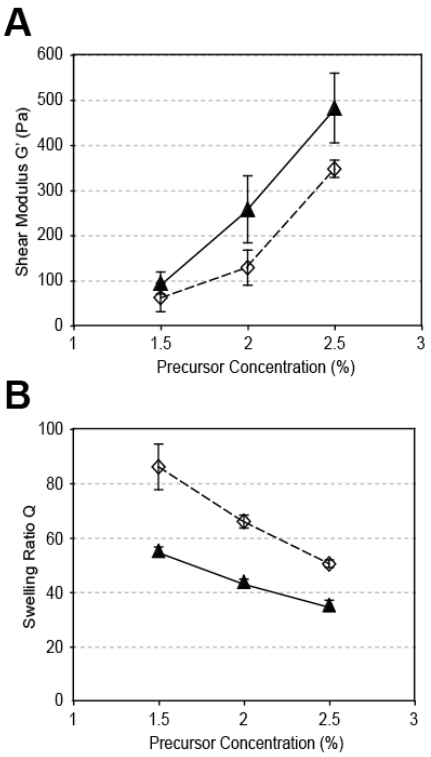

Figure S2. Physicochemical characterization of the chosen model aECMs. (**A**) The storage modulus G´ increased with increasing precursor concentration. MMP-degradable hydrogels are stiffer than MMP-insensitive gels formed at the same precursor concentration. (**B**) The swelling ratio Q decreased with increasing the precursor concentration. Notably, the MMP-insensitive hydrogels swelled consistently more than the MMP-sensitive gels. (mean ± SD, n = 5)

2. Measurement of sol fraction

The sol fraction of the gel networks formed at 1.5% was measured by RP-HPLC.

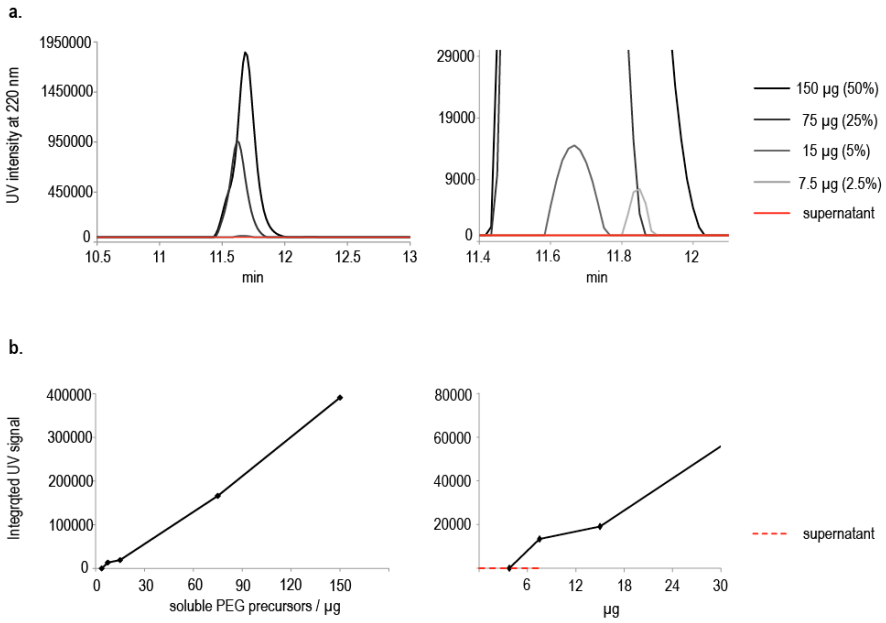

Figure S3. Evaluation of sol fraction. **(A)** chromatogram of different PEG-precursors concentrations (grey gradient) and analysis of 1.5% gel supernatant after swelling in water (ratio gel to water, 1:4) in red; **(B)** Standard curve of integrated UV signal obtained from chromatograms, showing that analyzed supernatant is below detection limits. Thus, we can afirm that any network defects would be negligible as they would be due to, at most, to 2.5% of the total gel mass remaining unreacted (and most likely less, but undetectable with our current methodology).

3. Influence of gel stiffness on 3D cell spreading

Single MC3T3-E1 murine pre-osteoblastic cells were encapsulated in degradable gels with variable stiffness and imaged by confocal microscopy after 24 hours in culture (**Fig. S4**). Cells in soft gels adapted a spindle-shaped morphology. With increasing stiffness the morphology became less elongated and reticulate filopodia were formed. In the stiff gels the cells remained almost round with frayed filopodia.

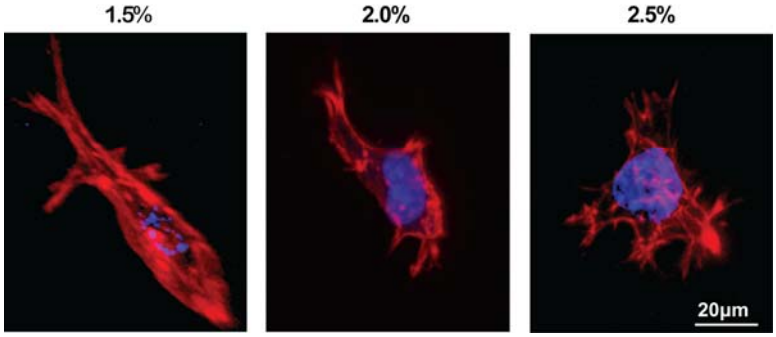

Figure S4. Typical confocal fluorescence images of spreading and elongating cells 24 hours after encapsulation of single cells in soft (1.5%), intermediate (2.0%), and stiff (2.5%) matrices. Rhodamine-phalloidin stained f-actin is shown in read and co-stained nuclei stained with DAPI are in blue.

4. The influence MMP inhibition on MC3T3-E1 cell migration

MC3T3-E1 cells were encapsulated in MMP-sensitive (**Fig. S5A**) and MMP-insensitive (**Fig. S5B**) hydrogels of different stiffness and, after initial swelling, immobilized on the bottom of tissue culture plates. In order to inhibit MMP activity, the cell culture medium was supplemented with 50 μM of the pan-MMP inhibitor GM6001. Whereas the migration of cells is blocked in intermediate and stiff MMP-sensitive gels, the migration in soft gels cannot be blocked by the inhibition of MMPs.

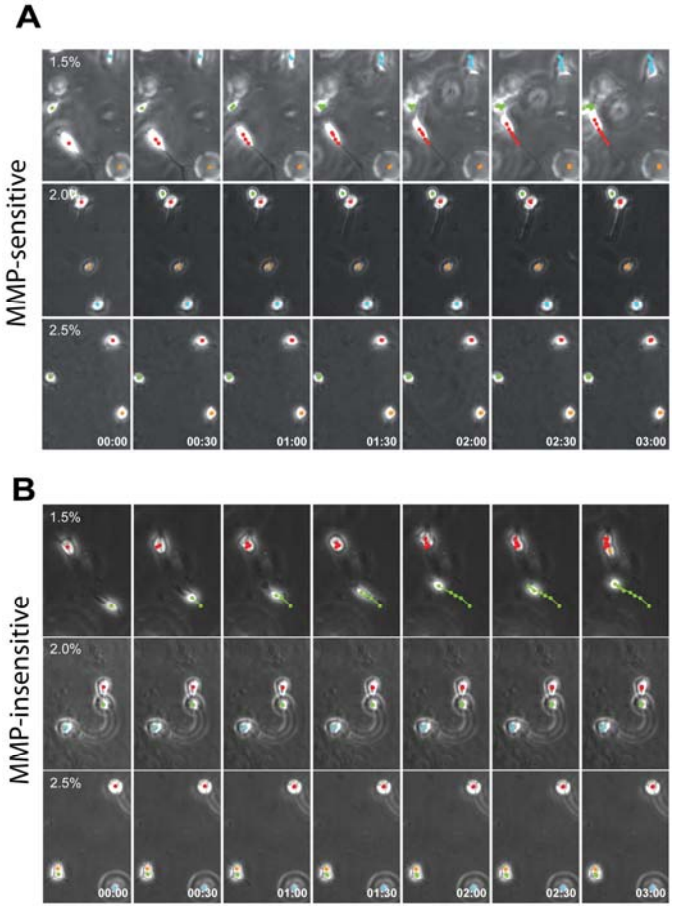

Figure S5. Representative Time-lapse images of MC3T3-E1 cells in 3D culture *in presence of MMP inhibitor GM6001* (time interval t = 30min.). Efficient migration in soft **(A)** MMP-sensitive and **(B)** MMP-insensitive hydrogels is observed, whereas the migration, but not sprout formation, is efficiently blocked by GM6001 in gels with higher stiffness.

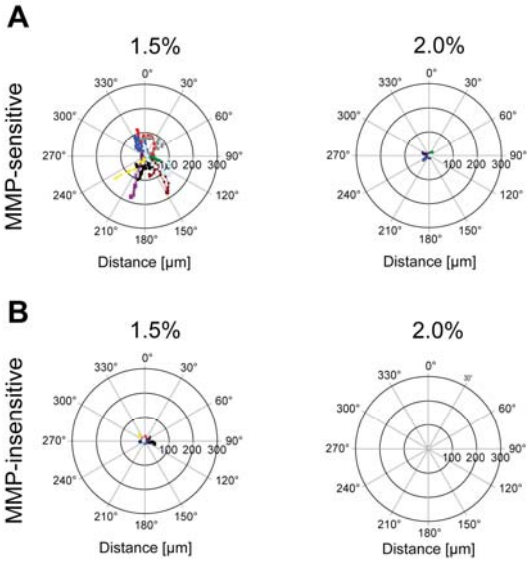

Figure S6. Representative track plots of MC3T3-E1 cells in 3D culture in presence of MMP inhibitor GM6001. The projection of 10 migrating cells was acquired and overlaid with a common starting point. The tracks representing a 14.5 hour period (58 x 15min.) do not show a preferred orientation. (**A**) Efficient migration in soft MMP-sensitive hydrogels is observed that is blocked at intermediate stiffness. (**B**) While some migration in soft MMP-insensitive hydrogels is observed the migration of cells in gels with intermediate stiffness is completely blocked by the MMP inhibitor.

5. Quantification of 3D single cell migration behavior

3D migration rate and persistence time based on time-lapse imaging series of at least 24 consecutive time frames were calculated using an unbiased random walk model (**Fig. S7**).

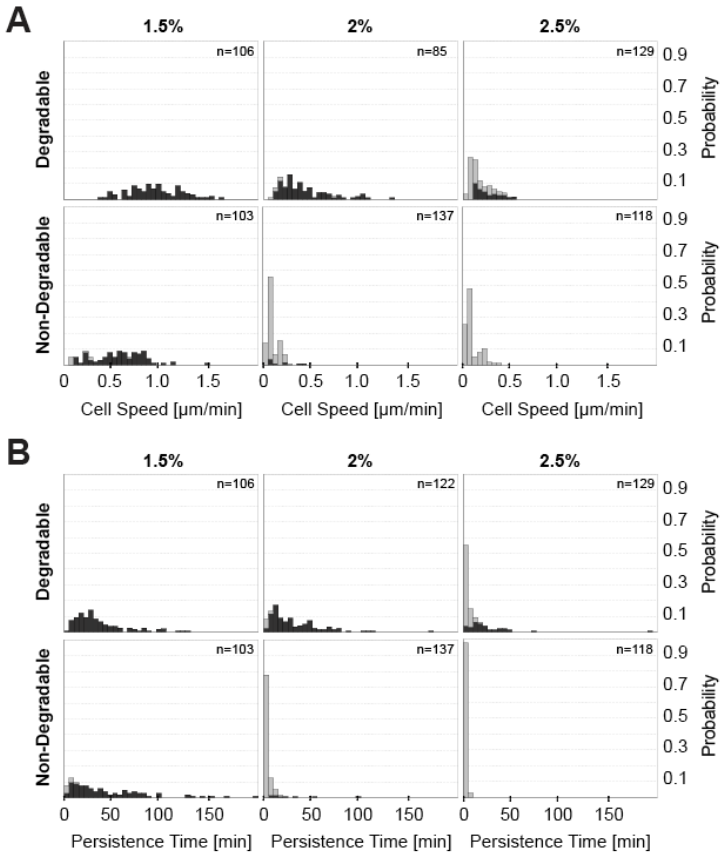

Figure S7. Migration parameters of 3D-encapsulated single cells. Cell tracks were assigned to migrating (black) or non-migrating (grey) groups, based on the persistence length criterion L_{crit}=1.2 µm. Histograms show the pooled data of three independent experiments with a total of *n* cell tracks. Depicted are **(A)** mean cell speed and **(B)** persistence time. The number of cells having a mean speed or a persistence time within a certain bin are divided by the total number of cells to give a normalized number indicated on the probability axis. Tracks with persistence time values derived from a regression analysis with R^2 <0.60 were excluded from the evaluation.

6. Determination of the migrating cell population

The percentage of migrating cells in MMP-sensitive gels decreased with increasing stiffness. (**Fig. S8**). In MMP-insensitive gels migration is only possible in soft gels and is completely blocked in intermediate and stiff gels.

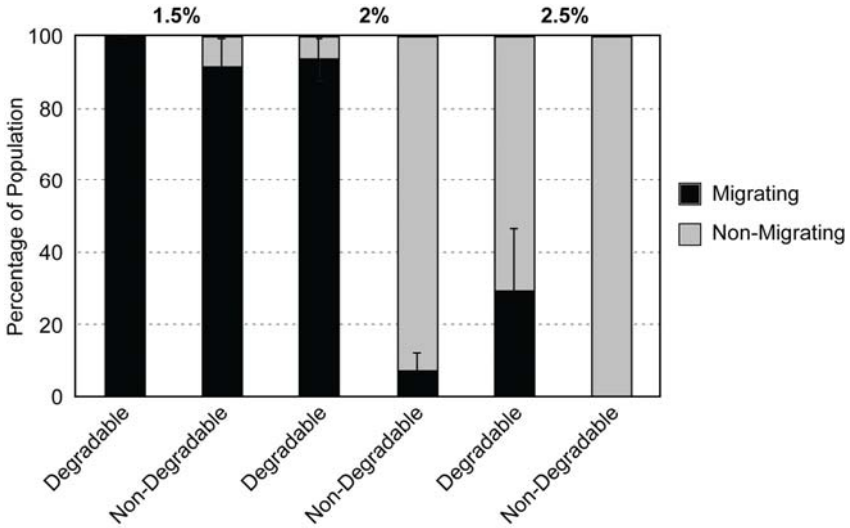

Figure S8. Migrating cell population of 3D encapsulated single-cells. Projections of 3D track were acquired with an inverse wide-field microscope and tracks were analyzed manually. After the evaluation of cell migration parameters persistence time and cell speed, cells were grouped in a migrating and non-migrating population based on the persistence length criterion L_{crit} = 1.2 μm. Each cell track was assigned to a migrating (black) or a non migrating (grey) group, based on the persistence length criterion L_{crit}=1.2 μm. All cells or almost all cell migrated in the soft gels that are MMP-sensitive or MMP-insensitive respectively. With increasing the stiffness to intermediate and stiff gels, the migrating population decreased in the MMP-sensitive gels. In the MMP-insensitive gels the migrating population was dramatically reduced in intermediate and completely absent in the stiff

7. Pan-MMP inhibitor GM6001 prevents the formation of cellular networks

Single cells cultured for three weeks in MMP-sensitive or MMP-insensitive gels form cellular networks. However migration is observed in these gels cellular network are not formed in presence of the MMP inhibitor (**Fig. S9**).

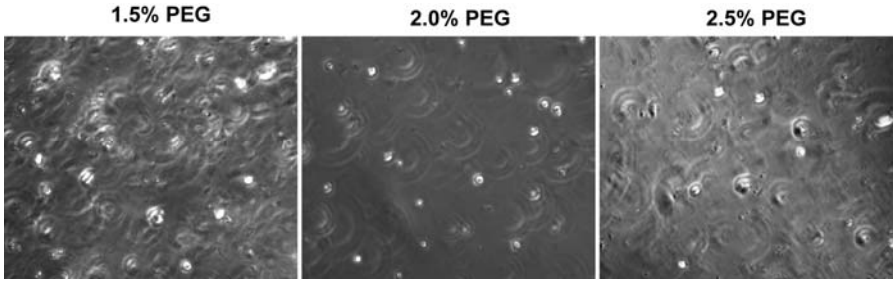

Figure S9. Cellular networks in MMP-sensitive matrices is absent in presence of MMP inhibitor. Cells that are encapsulated in soft degradable gels can migrate in presence of the MMP inhibitor GM6001. However they do not form cellular networks during the three weeks culture in presence of the inhibitor.

8. More detailed version of Materials and Methods

6.1 Material and Reagents

PEG-peptide conjugates Production and characterization of different eight-arm PEG precursors containing pending factor XIIIa substrate peptides having either a glutamine acceptor substrate (*n-PEG-Gln*) or a lysine donor substrate containing a MMP-sensitive linker (*n-PEG-MMP$_{sensitive}$-Lys)* or a MMP-insensitive linker *(n-PEG-MMP$_{insensitive}$-Lys)* was performed as described elsewhere (11). In brief, eight-arm PEG mol. wt. 40000 was purchased from Nektar (Huntsville, AL, USA). Divinyl sulfone was purchased from Aldrich (Buchs, Switzerland). PEG vinylsulfone (PEG-VS) was produced and characterized as described elsewhere (20). The factor XIIIa substrate peptides H-NQEQVSPL-ERCG-NH_2 (TG-*Gln*) Ac-FKGG-GPQGIWGQ-ERCG-NH_2 (*MMP$_{sensitive}$-Lys)* Ac-FKGG-GDQGIAGF-ERCG-NH_2 (*MMP$_{insensitive}$-Lys)*, Ac-FKGG-K-FITC (TG-*Lys-FITC)*, and the adhesion ligand Ac-GCYGRDGSPG-NH_2 (TG-*Gln-RGD*) were obtained from NeoMPS (Strasbourg, France) (immunograde, C_{18}-purified, HPLC analysis: > 90%). The NQEQVSPL cassette corresponds to the factor XIIIa substrate site in α_2-plasmin inhibitor (21), the FKGG cassette to an optimized factor XIIIa substrate site (22), and the ERCG cassette to the vinylsulfone-reactive Cysteine (23). In separate vials *TG-Gln, TG-MMP$_{sensitive}$-Lys or TG-MMP$_{insensitive}$-Lys* were added to PEG-VS in 1.2-fold molar excess over VS groups and allowed to react in 0.3 M triethanolamine (pH 8.0) at 37°C for 2 h. The products were dialyzed (Snake Skin, MWCO 10K, PIERCE, Rockford, IL, USA) against ultrapure water for 3 days at 4°C. After dialysis, the salt-free products (*8-PEG-MMP$_{sensitive}$-Lys, 8-PEG-MMP$_{insensitive}$-Lys* and *8-PEG-Gln*, respectively) were lyophilized to obtain a white powder. The peptide-PEG conjugation was confirmed via ^{1}H NMR.

6.2 PEG hydrogel preparation

100 µL of factor XIIIa (200 U/mL, a generous gift from Baxter BioSurgery, Vienna, Austria) was activated with 10 µL of thrombin (20 U/mL, Sigma-Aldrich, Switzerland) for 30 min at 37°C. Small aliquots of activated factor XIIIa were stored at -80°C for further use. Precursor solutions to give hydrogels with a final dry mass content of 1.5, 2.0 and 2.5% were prepared by stoichiometrically balanced ([*Lys*]/[*Gln*] = 1) solutions of *n-PEG-Gln* and *n-PEG-MMP$_{sensitive}$-Lys or n-PEG-MMP$_{insensitive}$-Lys* in Tris-Buffer (TBS, 50 mM, pH 7.6) containing 50 mM calcium chloride, leaving open a spare volume of 12.5% v/v for later addition of cell culture medium. The cross-linking reaction was initiated by 10 U/mL thrombin-activated factor XIIIa and vigorous mixing, immediately followed by addition of 12.5% v/v cell culture medium with or without cells. To obtain disc-shaped matrices, the liquid reaction mixtures (20 - 40 µL) were sandwiched between sterile hydrophobic glass microscopy slides (obtained by treatment with SigmaCote, Sigma) separated by spacers (ca. 1 mm thickness) and clamped with binder clips. To prevent sedimentation of cells, the forming matrices were slowly rotated for 10min. at RT (until the onset of gelation) and then incubated for additional 30min. at 37°C.

6.3 PEG hydrogel characterization

Rheometry on swollen gels. Storage and loss moduli (G' and G") of swollen gels were obtained by small strain oscillatory shear rheometry (20). Briefly, swollen hydrogel discs of 1 to 1.4 mm thickness were sandwiched between the two plates of the rheometer with compression up to a range between 85% to 75% of their original thickness to avoid slipping.

Measurements were then conducted in a constant strain (0.05) mode as a function of frequency (from 0.1 to 10 Hz) to obtain dynamic mechanical spectra (n=4 per condition).
Equilibrium swelling measurements. Swollen hydrogels were weighted just prior to rheometry, and the swelling ratio Q determined as the swollen gel mass divided by the gel's dry mass (calculated from the reaction conditions).
Detection of sol fractions by HPLC. The potential presence of defects in the network architecture due to uncrosslinked PEG precursors was investigated by reverse phase high-performance liquid chromatography (RP-HPLC). First, a dilution series of unreacted PEG precursors was run on an RP-HPLC instrument using a Waters (Milford, MA, USA) C_{18} symmetry column in order to establish a standard curve of UV intensities (recorded at 220nm) as a function of PEG concentration. Then, gels (50µl volume formed at 1.5% w/v) were prepared (n=4) and each was incubated in 200µl water for 24 hours. The supernatant was then collected, run on the HPLC instrument and UV intensities were compared to the standard curve to determine the corresponding amount of unreacted polymer remaining in solution.

6.4 Cell culture

Mouse preosteoblastic cells MC3T3-E1 were purchased from American Type Culture Collection (ATCC) and grown under in MC3T3-E1 culture medium (alpha-minimal essential medium, with 10% fetal bovine serum, 100U/ml penicillin G and 100mg/ml streptomycin GIBCO BRL, Life Technologies, Grand Island, NY, USA) under standard cell culture conditions (37°C in humidified atmosphere and 5% CO_2).

6.5 Cell encapsulation

Cells suspended in cell culture medium were added right after the FXIIIa enzyme to yield single dispersed cells at a final seeding density of 6 x10^4 cells / ml of hydrogel. Subsequently the forming matrices were slowly rotated (10min at RT) until the onset of gelation to prevent sedimentation of cells, then incubated at 37°C and 5% CO_2 for additional 30 min. and finally immersed in cell culture medium

6.6 Cell migration assay

Cell migration experiments were conducted at 37°C and 5% CO_2 and high relative humidity. Hydrogel discs containing dispersed cells were equilibrated for 4 hrs in cell culture medium and then 'glued' to the bottom of 24 well cell culture dishes by applying 10 µl of 5% hydrogel to the edge of the discs. After gelation was allowed to take place for 30 min, the samples were equilibrated for 1 hour in 1 ml of pure cell culture medium or medium that contained 50µM of the broad-range MMP inhibitor GM6001 (Chemicon). Three random (x-y-z) positions, carefully selected to be completely inside the matrix, were selected using an inverse wide-field microscope (Leica, DM IRBE) equipped with a motorized stage and focus, and a black and white camera (Hamamatsu ORKA ER). Cell spreading and migration was followed for up to 36 hours by software-controlled image acquisition (Openlab) every 15 minutes.

6.7 Statistical analysis of migration parameters

Projections of real 3D tracks were followed manually by using a "Manual Tracking" plugin in ImageJ software. The resulting x and y coordinates were used in a correlated random walk model, as described by Raeber et *al.* (17). This model assumes that the cell velocity decays exponentially with time with a characteristic time constant P (directional persistence time).

Thus the mean-squared displacement of a cell during the time interval Δt is related to P and the root mean squared speed S by the equation which applies for cells migrating on 2D as well as in 3D:

$$<d^2(t)> = 2S^2P[t-P(1-e^{-t/P})] \quad (1)$$

Consistent with our earlier work, we observed no preferential migration direction when the distance was plotted against the direction in a polar plot (Fig. 3A and Supplemental Fig. 2) (17). Therefore for such isotropic migration, the projected cell speed S_{2D} was corrected by a geometry factor of sqrt(3/2) to give an estimate of S. The mean-squared displacements $<d^2(t)>$ from experimental cell-track data were calculated by the method of overlapping intervals and corrected to predict the 3D displacement from the 2D projections. The dimension-corrected cell speed S was used as an input parameter to fit Eq. 1 to the dimension-corrected displacement data by a nonlinear least-square regression analysis to obtain an estimate of the directional persistence time P. The persistence length L was defined as the product L = P x S. The S and P values of individual cell tracks from the same treatment and three independent experiments were pooled to generate cell-population histograms and box plots extending from the 25th to the 75th percentile, including the median, whiskers from the 10th to the 90th percentile, and a symbol corresponding to the arithmetic mean. Tracks with persistence time values derived from regression analysis with $R^2 \leq 0.6$ were excluded from the study. Homogeneity of variances and normality of errors was not given for migration parameters. For statistical analysis, multiple comparisons were therefore conducted with the Dunn's test, a nonparametric rank sum test suitable for unequal sample sizes. In an additional analysis the whole cell populations was divided, based on the persistence length criterion $L_{crit} \leq 1.2$ μm as a threshold, into a motile (persistence length $L \geq L_{crit}$) and a non-motile fraction. Since we were interested in cell motility in hydrogels with different compositions, this criterion allowed us to discriminate between cells that oscillated in cavities developed during the gelation process and cells that effectively migrate.

6.8 Staining and confocal microscopy

MC3T3-E1 cells were stained for f-actin and nuclei. Samples were fixed and permeabilized in 4% paraformaldehyde containing 0.2% Triton X-100 in PBS for 20 min at 4°C. Samples were incubated for 10 min in 0.1 M glycine followed by a wash step in PBS. For f-actin staining, the gels were incubated with 0.4 U/ml rhodamine-labeled phalloidin (R-415; Molecular Probes, Eugene, OR, USA) in PBS with 1% BSA for 1 h at 4°C. After washing the samples three times for 5 min in PBS, cell nuclei were co-stained with 1 ng/μl DAPI (4',6-diamidino-2-phenylindole) (D-1306; Molecular Probes, Eugene, OR, USA) in PBS for 10 min at 4°C. Z-series of approximately 30 equidistant x-y scans at 0.272 μm intervals (63x) were acquired and processed in Imaris software (Bitplane AG, Zürich, Switzerland).

For time-lapse confocal imaging, cells were stained with PKH-26 (Sigma-Aldrich) according to the manufacturer's instructions. Fluorescently labeled cells were encapsulated in hydrogels containing covalently linked TG-Lys-FITC (24). The resulting hydrogel discs were equilibrated for 4hrs in cell culture medium and then glued to the bottom of 24 well cell culture dishes by applying 10 μl of 5% hydrogel to the edge of the discs. Z-series of approximately 100 equidistant x-y scans at 1.5 μm intervals (20x) were acquired for 8 hours at 15 min. intervals in resonant scanning mode with a Leica TCS SP5 confocal microscope and processed in Imaris software.

6.9 Animal experiments

Animal experiments were authorized by the Veterinary Authority of the Canton of Zurich. Adult female Sprague-Dawley albino rats (300-350 g) were used for bone regeneration experiments as previously described (25). Briefly, an 8 mm calvarial defect was created in the parietal bone with a dental handpiece. After removal of the calvarial disk, bone debris were removed by rinsing the surgical site. Preformed hydrogel disks (8 mm diameter and 1 mm in thickness) were placed into the defect. After two weeks, the animals were sacrificed and explanted skulls were fixed with 4% formalin before decalcification in UsedecalcậMedite), Nunningen, Switzerland). 5 mm paraffin sections were taken through the centre of the implantation site and, after staining with Hematoxylin and Eosin, composite images were generated with a 5x objective on a Leica DM 5500B microscope. For the quantitative evaluation of gel leftovers, images were superimposed onto a grid of 88 points/mm^2. The number of test points covering the remaining gel mass were counted and standardized against sections derived from gels that were not implanted. Four to five animals were used per gel type.